Vibrational coherences in manganese single-molecule magnets after ultrafast photoexcitation

Florian Liedy[1], Robbie McNab[1], Julien Eng[2], Ross Inglis[1], Tom J. Penfold[2], Euan K. Brechin[1], J. Olof Johansson[1,*]

[1]*EaStCHEM School of Chemistry, University of Edinburgh, David Brewster Road, EH9 3FJ, Edinburgh, UK*

[2] *Chemistry - School of Natural and Environmental Sciences, Newcastle University, Newcastle upon Tyne, NE1 7RU, UK*

**Email: olof.johansson@ed.ac.uk*

Abstract

Single-Molecule Magnets (SMMs) are metal complexes with two degenerate magnetic ground states arising from a non-zero spin ground state and a zero-field splitting. SMMs are promising for future applications in data storage, however, to date the ability to manipulate the spins using optical stimulus is lacking. Here, we have explored the ultrafast dynamics occurring after photoexcitation of two structurally related Mn(III)-based SMMs, whose magnetic anisotropy is closely related to the Jahn-Teller distortion, and demonstrate coherent modulation of the axial anisotropy on a femtosecond timescale. Ultrafast transient absorption spectroscopy in solution reveals oscillations superimposed on the decay traces with corresponding energies around 200 cm^{-1}, coinciding with a vibrational mode along the Jahn-Teller axis. Our results provide a non-thermal, coherent mechanism to dynamically control the magnetisation in SMMs and open up new molecular design challenges to enhance the change in anisotropy in the excited state, which is essential for future ultrafast magneto-optical data storage devices.

Single-Molecule Magnets (SMMs), molecules that show magnetic hysteresis below a certain blocking temperature[1], show great promise for future applications in data storage devices[2-4] because their small size and well-defined magnetic properties can reduce the size of data bits and therefore increase storage density. The recent observations of hysteresis loops close to[5,6], or above[7], liquid nitrogen temperatures (77 K) in lanthanide-based SMMs provide an important step forward, but to implement these molecules in devices methods to control the spins need to be developed. Being able to switch the magnetisation direction in SMMs using femtosecond laser pulses could provide the technology for future ultradense memory devices operating on unprecedented timescales. Because the slow magnetic relaxation in SMMs means that they can retain the magnetisation direction for months[1], spin-switching in SMMs is advantageous over spin-crossover (SCO) switching in paramagnetic Fe(II) complexes, even though SCO is well studied and known to occur on ultrashort timescales[8-12]. Light-induced SCO can result in SMM properties in some crystals but on timescales from minutes to hours[13,14], which is too slow for applications. Despite this potential, there are a limited number of studies of ultrafast dynamics in molecule-based magnets. For example, ultrafast charge-transfer dynamics[15], phase-transitions[16] and intersystem crossing[17] have been studied in magnetic Prussian blue analogues, and spin state switching has been observed in Cu(II)-based breathing crystals[18]. Magnetic nanotoruses have been studied using transient absorption (TA), identifying lanthanides as trap states for excitons[19]. In this work, we have developed a detailed understanding of the ultrafast photophysics of Mn(III)-based SMMs and prove that coherent vibrational wavepackets modulate the Jahn-Teller (JT) axis, and therefore the magnetic anisotropy, on an ultrafast timescale.

Manganese-based coordination complexes, such as Mn_{12}[20,21], have been instrumental in the development of SMMs and are typically magnetically bistable due to a large, negative zero-field splitting caused by the magnetic anisotropy of individual Mn(III) ions. The $3d^4$ electron configuration leads to an elongation or compression of the axial bonds via the JT distortion. Together with the spin-orbit interaction, this leads to two degenerate magnetic ground states

where the ground state spin is saturated either parallel or anti-parallel to the magnetic easy axis. Transiently reducing the anisotropy in SMMs, using femtosecond laser pulses, could provide a method towards achieving optical control of their magnetisation, making use of quantum coherences that can be created using ultrashort laser pulses[22]. The prototype Mn-based SMM $Mn_{12}Ac$ (Ac = acetate) is promising for exploring optical modulation of the anisotropy because it has been shown that reorienting the JT axis with high pressure can strongly influence the molecules magnetic properties[23]. Similarly, there have been reports of ultrafast spin-switching of Cu(II) molecule-based magnets due to optical modulation of the JT axis[18,24]. However, said species are large and structurally complex, with smaller molecules being better suited to achieving a more detailed understanding of the photophysics. One such example is a family of oxime-based SMMs containing three or six Mn(III) ions whose magneto-structural relationship has been extensively investigated[25-29]. Herein, we present ultrafast transient absorption spectroscopy of $[Mn(III)_3O(Et\text{-}sao)_3(b\text{-}pic)_3(ClO_4)]$, or "$Mn_3$", which has three high-spin Mn(III) ions arranged in a simple triangle[26] (Figure 1**A**) and $[Mn(III)_6O_2(Et\text{-}sao)_6(O_2CPh(Me)_2)_2(EtOH)_6]$, or "$Mn_6$", which contains six high-spin Mn(III) ions arranged in two triangles[30] (Figure 1**B**). We show that photoexcitation leads to a change in the JT distortion and that a coherent wavepacket is launched towards the new equilibrium bond length on the excited state potential energy surface for both Mn_3 and Mn_6. The structural rearrangements and a dephasing of the vibrational wavepacket take place on a sub-ps timescale. The excited electronic state decays back to the ground electronic state with a decay constant of 8 – 9 ps for both molecules studied. These measurements reveal, for the first time, the possibility to coherently control both the anisotropy and the exchange interaction in SMMs on the femtosecond timescale.

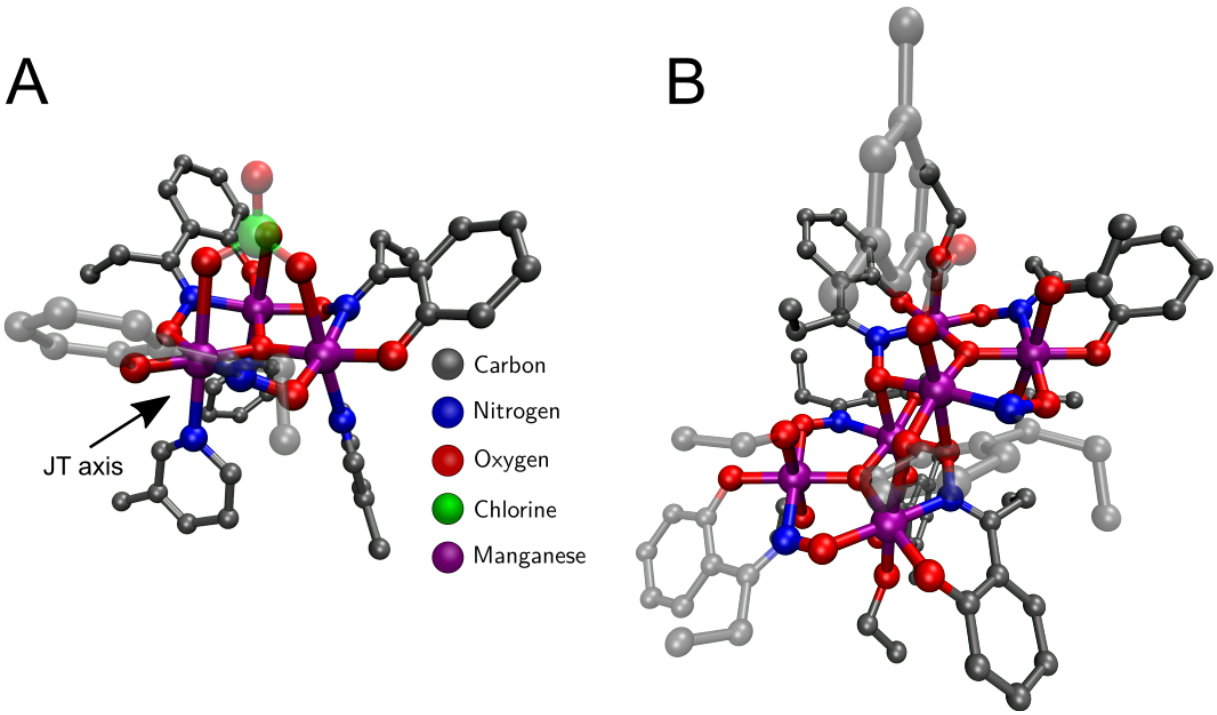

Figure 1 Structure of the Mn-based SMMs used in this study. *Crystal structures of* ***A*** *Mn_3 and* ***B*** *Mn_6. Manganese = purple; carbon = grey; oxygen = red; nitrogen = blue; chlorine = green. The hydrogen atoms are omitted for clarity.*

Results

Static UV/ Vis absorption spectroscopy

Static UV/Vis absorption spectra of both manganese complexes (Figure 2**A**) show almost identical absorption bands (which are also similar to the Mn_{12} spectrum[31-34]). In the visible region, the spectra are rather unstructured although one weak shoulder at 375 nm can be discerned. MCD measurements by Bradley *et al.*[28] showed that metal-centred transitions are responsible for the absorption above 410 nm. In the ultrafast TA measurements, 400 nm light was used for excitation. This spectral region is tentatively assigned to charge-transfer (CT) transitions due to the large molar absorptivity observed (Figure 2**A**). Ligand-centred ππ* transitions on the salicylaldoxime ligand show no absorption below 400 nm[35]. The CT transitions are most likely due to ligand-to-metal CT (LMCT), transiently reducing the Mn(III) to Mn(II). However, due to the low symmetry of the molecules, the degeneracy is completely

lifted and metal-centred transitions with non-zero extinction coefficients are also expected[36 28 32]. We therefore assign the 375 nm shoulder to a mixture of LMCT transitions and spin-allowed d-d transitions, although CT transitions will most likely dominate due to the larger oscillator strength.

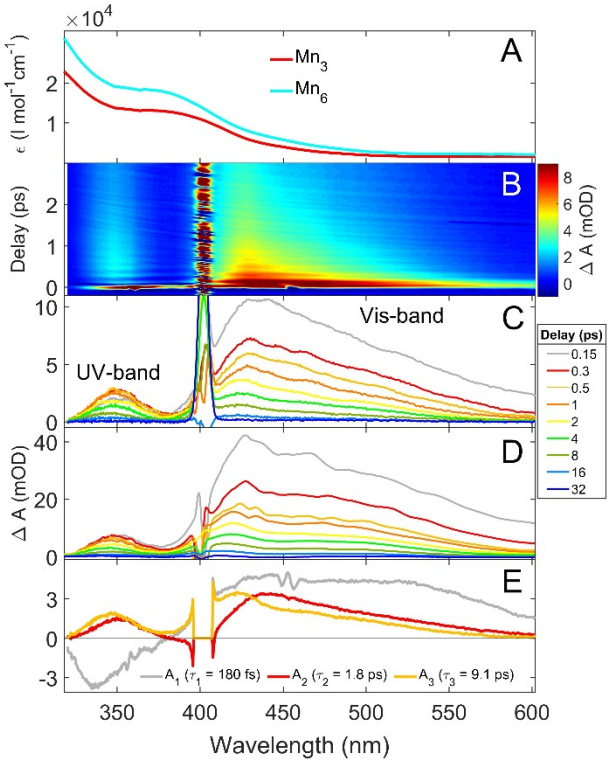

Figure 2: Static UV/Vis absorption and ultrafast transient absorption of Mn-based SMMs. A *Static absorption spectra of the Mn_3 and Mn_6 complexes in ethanol showing the molar absorptivity ε as a function of wavelength.* ***B*** *Contour plot of the transient absorption (TA) data of Mn_3 after pumping at 400 nm. The pump-probe delay is plotted against the wavelength and the colour code indicates the absorbance change (ΔA). Difference spectra ΔA for selected time delays from the TA data in ethanol after pumping at 400 nm are shown in* ***C*** *for Mn_3 and* ***D*** *for Mn_6. The sharp features around 400 nm in* ***B*** *–* ***D*** *are due to scattered pump light.* ***E*** *Decay associated spectra (DAS) of the Mn_3 data set obtained after a global fit using a sequential tri-exponential fit model, where the pre-exponential factors A and their corresponding time constants are shown in the legend. The 180 fs timescale is just within our temporal resolution and so the DAS are influenced by the difficulties with correctly removing the cross-phase modulation.*

Transient absorption

In Figures 2**B – D**, the difference spectra for selected time delays of the TA are shown. The difference spectra for both Mn complexes are similar. Two positive bands, due to excited state absorption (ESA), are observed around 350 nm ("UV-band") and 430 nm ("Vis-band"). The Vis- and UV-bands are broad and are probably comprised of several unresolved peaks. In fact, the Vis band can be seen to separate into two bands at longer time delays with maxima at *ca*. 420 and 500 nm. However, the decay kinetics are very similar for the two sub-bands and because they cannot be resolved at earlier times, we treat them as one ("Vis band"). The maxima of both the UV- and Vis-bands are shifted towards shorter wavelengths for longer time delays for both molecules. Furthermore, the maximum of the Vis-band of Mn_6 is blue shifted in relation to Mn_3 for pump-probe delays longer than 0.5 ps.

Kinetic traces of the TA measurements at two different wavelengths for both Mn complexes are shown in Figure 3 (further kinetic traces can be found in Figure S2). The 440 nm kinetic trace shows a fast decay during the first few ps and a slower decay back to zero in ~20 ps. This is observed for both Mn_3 and Mn_6. For the 345 nm trace, a very fast initial rise of the absorption change is observed for Mn_3 (Figure 3**E**). The rise is not observed at 345 nm for Mn_6 (Figure 3**G**), although can be discerned at shorter wavelengths (Figure S1**B** and S2**E**). After reaching the maximum absorption change, the UV-bands for both molecules decay back to zero on a similar timescale as the Vis-bands. The Glotaran software[37] was used for a sequential global analysis of the whole data set, which took into account the instrument response function and cross-phase modulation at time-zero. Three exponential decays were needed to obtain a good fit, with corresponding pre-exponential factors A_x and time constants τ_x (x = 1,2,3). For Mn_3, a fast decay constant of τ_1 = 180 ± 10 fs was found and for Mn_6 τ_1 = 70 ± 10 fs was found (70 fs is below our temporal resolution). An intermediate time regime was τ_2 = 1.8 ± 0.2 ps for Mn_3 and τ_2 = 1.0 ± 0.3 ps for Mn_6. The longer time constants were τ_3 = 9 ± 1 ps for Mn_3 τ_3 = 8 ± 1 ps for Mn_6. The decay-associated spectra (DAS), corresponding to the spectral dependence of A_x, for Mn_3 are shown in Figure 2**D**. The fast initial 180 fs

component is dominated by ESA in the visible region and is broader and red-shifted compared to the main Vis band dominating the signal in Figures 2**B** – **D**. In addition, the UV region shows a negative amplitude at these time delays, possibly due to ground-state bleach (GSB).

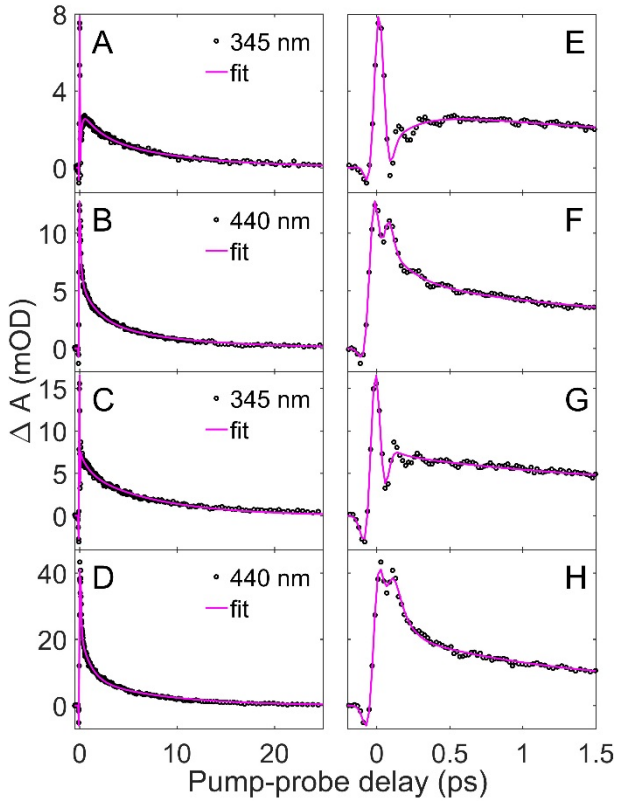

Figure 3: Ultrafast transient absorption of Mn-based SMMs. *Kinetic traces at* ***A*** *345 nm and* ***B*** *440 nm for* Mn_3*. The corresponding data for* Mn_6 *are shown in* ***C*** *and* ***D****. The tri-exponential sequential fits for the data are shown as solid magenta lines. The following time constants were obtained for* Mn_3*:* $\tau_1 = 180 \pm 10$ *fs,* $\tau_2 = 1.8 \pm 0.2$ *ps and* $\tau_3 = 9 \pm 1$ *ps, and for* Mn_6*:* $\tau_1 = 70 \pm 10$ *fs,* $\tau_2 = 1 \pm 0.3$ *ps and* $\tau_3 = 8 \pm 1$ *ps. Panels* ***E – H*** *show early pump-probe delays of the plots* ***A – D****, where the cross-phase modulation and the oscillations can be observed.*

Wave packet dynamics

We clearly observe oscillations superimposed on the transient absorption signals during the first picosecond across the two ESA bands (Figure 3**E** – **H**). In Figure 4, averages over a small wavelength region, corresponding to ca. 1000 cm^{-1}, of the residues from the global tri-exponential fit of the Vis- and UV-bands are shown. The Fourier analysis of the fit residues are shown in Figure 5**A**. We found that the frequency spectrum is mainly composed of one dominant peak for both Mn complexes, with peaks centred at 172 cm^{-1} (177 cm^{-1}) for the Mn_3 Vis-band (UV-band) and 189 cm^{-1} (201 cm^{-1}) for Mn_6 Vis-band (UV-band). We have also performed Raman spectroscopy on crystal grains of the molecular solids to compare the vibrational spectra to the oscillations observed in the transient absorption. The resulting spectra are shown in Figure 5**B**. The Raman spectra for the two molecules are rather similar, although the peaks are somewhat broader for Mn_6. However, some of the peaks are shifted, and interestingly, the largest shift is for the intense peaks at 213 cm^{-1} and 191 cm^{-1} for Mn_3 and Mn_6, respectively. These are in the same region as the ones found in the Fourier analysis of the TA data. We also performed a DFT analysis to calculate the Raman spectrum of Mn_3 (Figure 5**C**). The calculated Raman spectrum agrees well with the measured one. In particular, the peak position in the calculated spectrum at 210 cm^{-1} fits very well to the measured peak at 213 cm^{-1}. This mode can be described as a collective in-phase asymmetric stretch mode along the JT axis for all three Mn ions (a video can be found in the SI), where the Mn–O bonds are contracted while the Mn–N bonds are extended and there is a flattening of the Mn triangle.

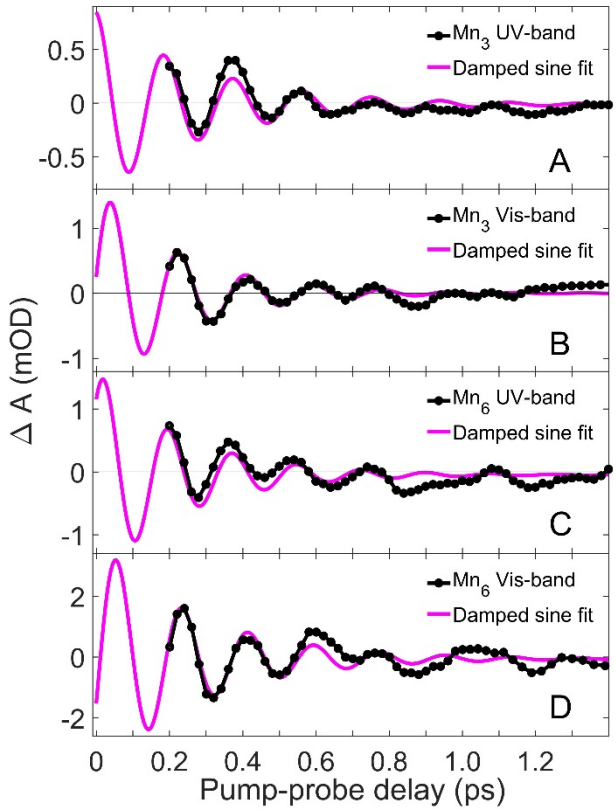

Figure 4 Damped oscillations in the TA data*. The average of the residues of a tri-exponential fit in the range* ***A*** *from 346 nm to 357 nm (ΔE = 891 cm^{-1}) for the Mn$_3$ UV-band,* ***B*** *from 415 nm to 435 nm (ΔE = 1108 cm^{-1}) for the Mn$_3$ Vis-band,* ***C*** *from 344 nm to 357 nm (ΔE = 1059 cm^{-1}) for the Mn$_6$ UV-band and* ***D*** *from 413 nm to 433 nm (ΔE = 1118 cm^{-1}) for the Mn$_6$ Vis-band. An average over a finite bandwidth was used to enable the observation of the oscillations for longer time delays, which improved the frequency analysis of the oscillations. The signal has been fitted with a damped sine-function to highlight that they are mainly composed of one frequency component. The periods of the fits are 185 ± 6 fs (189 ± 3 fs) for the Mn$_3$ Vis-band (UV-band) and 180 ± 6 fs (176 ± 10 fs) for the Mn$_6$ Vis-band (UV-band). An exponential damping function was fitted and the damping time constants were 231 ± 55 fs (293 ± 100 fs) Mn$_3$ Vis-band (UV-band) and 272 ± 65 fs (238 ± 100 fs) for the Mn$_6$ Vis-band (UV-band). The cross-phase modulation at time zero of the experimental data has hindered the determination of the exact phase of the oscillations. It has been removed for clarity.*

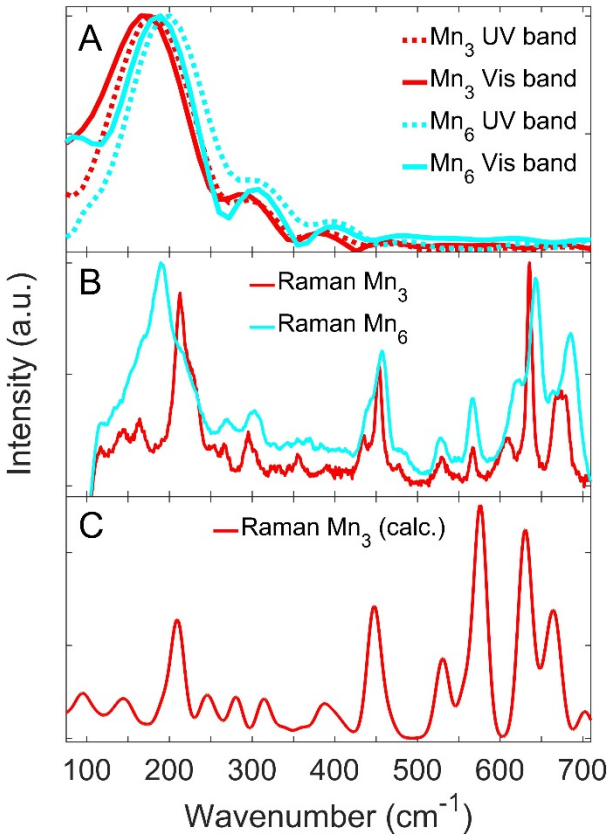

***Figure 5 Vibrational wavepacket**. **A** Fast Fourier transformation of the average residues of a tri-exponential fit for the Vis- and UV-bands from the data in Figure 4. We found wavenumbers of 172 cm^{-1}(177 cm^{-1}) for the Mn_3 Vis-band (UV-band) and 189 cm^{-1} (201 cm^{-1}) for the Mn_6 Vis-band (UV-band). **B** Raman spectra for the Mn_3 and Mn_6 complexes obtained from exciting crystal grains non-resonantly at 785 nm. **C** Calculated Raman spectrum of Mn_3.*

Discussion

The static absorption spectra of the two complexes show similar bands, which indicates that the optical transitions are to some extent localised, such as LMCT between O/N and Mn or d−d transitions, as previously discussed. The TA results are also similar, which is perhaps not surprising if the excitation is dominated by CT between specific Mn−O/N sites in the molecules. From the transient absorption data for both complexes we extract three time-constants in a sequential decay model. The first time constant is faster than 200 fs for both molecules and the corresponding DAS for this timescale are significantly different to the DAS for the two other timescales (ca. 1-2 and 8-9 ps), both of which show similar spectra with the characteristic UV-

and Vis-bands. The A_1 spectrum in Figure 2**E** therefore corresponds to the absorption from the initially excited LMCT state, which absorbs predominantly in the visible spectral region. The lack of absorption in the UV region allows for the GSB to be observed in this short timescale. The A_2 and A_3 DAS are different to A_1, which implies that there is a change in the electronic character of the excited state[38] and therefore an intermediate state is populated on a <200 fs timescale through internal conversion (IC) either within the LMCT manifold or via back-electron transfer into a metal-centred excited state.

We argue below that key to interpreting our results comes from realising that the molecules have a strong JT distortion, which introduces axial anisotropy in the system, perpendicular to the plane of the triangle formed by the three Mn(III) ions (Figure 1). One can therefore envisage ESA transitions whose transition dipole moments lie either equatorial (in-plane) or axial (out-of-plane) with respect to the triangle (or triangles in the case of Mn_6). The bond length between the Mn and the axial oxygen, connecting the two triangles, is 243 pm. This is much longer than the equatorial Mn−O bonds of 190 pm. The bond strength is therefore considerably weaker along the JT axis than the in-plane bonds. A CT transition into the d-orbitals will induce a change in the charge distribution in the molecule and consequently the JT distortion will be released, which was recently observed in perovskite manganites[39-41]. The release of the JT distortion via the mode identified by the DFT calculations causes a contraction of the axial Mn–O bonds. However, because the equatorial bonds are more restricted due to the larger bond strengths, we observe a larger change in the bond length along the JT axis. Because of the change in the bond lengths, ESA transitions will be affected by the different ligand-proximity to the Mn centres, and therefore the oscillator strength of the ESA will be modulated. Importantly, this effect will be larger for axial transitions than for equatorial transitions, since the bond length change is smaller in the latter case.

There are several experimental observations that point towards a large motion along the JT axis. By comparing the Mn_3 and Mn_6 results, we can gain some insights into any out-of-plane dynamics because the second triangle in Mn_6 enforces some constraints on the axial motion

in either triangle (Figure 1). The Vis-band peak maximum in the DAS for Mn_6, for both A_2 and A_3 (Figure S1**B**), is blue-shifted with respect to the peak positions in the Mn_3 DAS (Figure 2**E**) by 290 cm^{-1} for A_2 and 260 cm^{-1} for A_3. In contrast, there is no observable change in the peak position for the UV-bands. We therefore argue that the Vis-band arises from ESA transitions with axial transition dipole moments whereas the UV-band arises from transitions with equatorial transition dipole moments. We observe in the kinetics for both molecules that the magnitude of the change is larger for the Vis-band than the UV-band, as seen in Figure 3. This therefore also points towards a much larger change in bond lengths for the axial bonds than the equatorial bonds, due to the dependence of the oscillator strength on ligand-proximity. We therefore conclude that the JT distortion is indeed relaxed after exciting at 400 nm.

After the sudden release of the JT distortion, a fast motion out of the Franck-Condon region takes place towards the new bond length in the excited state. The fast motion occurs via the formation of a wavepacket involving quanta of a specific vibrational mode. The wavenumber of the wavepacket coincides with the observed strong Raman modes around 200 cm^{-1} in Figure 5**B**, although it is somewhat smaller because of weaker bonds in the excited state. The peaks at 200 cm^{-1} in the Raman spectra are strongly shifted for the two molecules, in contrast to the other Raman peaks in the spectra (Figure 5**B**). There is therefore a difference in vibrational energy when there is one (Mn_3) or two (Mn_6) triangles in contact with each other (Figure 1). Therefore, it can be concluded that the vibrational motion involves the out-of-plane JT axis. The other peaks in the Raman spectrum are localised to Mn−O or Mn–N bonds, where it does not matter if there is another Mn triangle in the proximity. The DFT calculations do indeed demonstrate a collective in-phase motion of the Mn ions along the JT axis (Figure 6**B** and supplementary video).

The dephasing of the wavepacket takes place on a longer timescale (ca. 300 fs) than the lifetime of the initially populated LMCT state and therefore survives the IC into the intermediate electronic state. The 1-2 ps decay constants can be assigned to vibrational cooling via intramolecular vibrational redistribution (IVR), which leads to the observed dephasing of

the wavepacket. The vibrational cooling can be inferred from the spectral narrowing and blue-shift in the absorption peak, as observed in Figure 3. The faster LMCT state decay and IVR in Mn_6 is due to a higher density of states than in Mn_3. Since the DAS for the 8-9 ps decay is similar to the 1-2 ps DAS, we argue that this corresponds to the decay of the vibrationally cool intermediate state back to the ground electronic state via IC. The photophysics model is summarised in Figure 6.

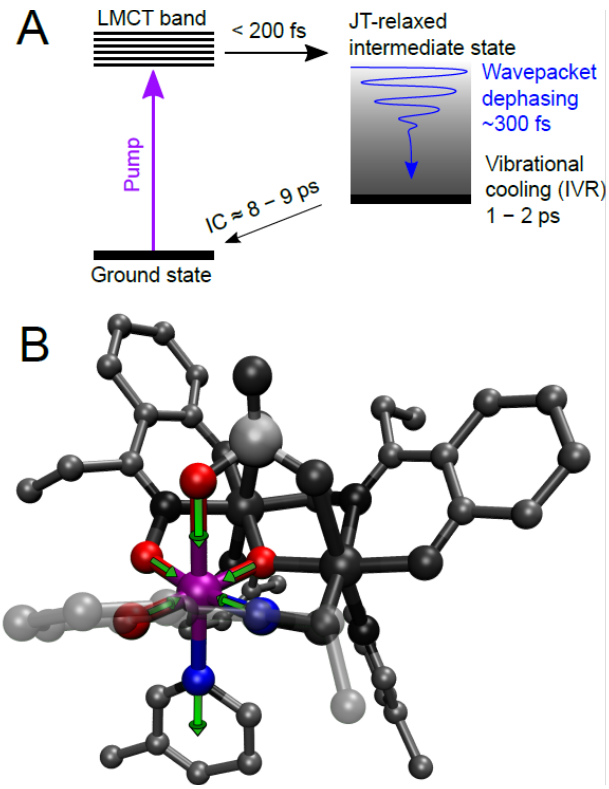

Figure 6 A Jablonski diagram for the dynamics in Mn_3 and Mn_6. *After exciting with 400nm, 120 fs laser pulses into the LMCT band, a fast decay via internal conversion (IC) takes place into an intermediate state, which leads to a vibrational wavepacket. The wavepacket dephases on a time scale of around 300 fs due to intramolecular vibrational redistribution (IVR) in the intermediate state, which in turn occurs in 1-2 ps. The electronic ground state is formed with a 7-9 ps decay constant.* ***B*** *Illustration of the vibrational mode of the wave packet. The main movement is a collective in-phase oscillation of the bond lengths along the JT axis for all three Mn ions, where the equatorial ligands bond lengths adjust accordingly. When the bond length*

of the JT axis nitrogen is stretched (JT oxygen bond length is shortening), the equatorial ligands also stretch, and vice versa. The atomic displacements are shown in the video in the SI.

Conclusions

In summary, we have performed transient absorption spectroscopy of Mn_3 and Mn_6 SMMs in ethanol at room temperature. We observed two characteristic ESA bands at ca. 345 and 430 nm after exciting with 400 nm light. We found oscillations superimposed on the decay signals, which were attributed to a vibrational wavepacket. By comparing the peak position of the ESA, decay dynamics, and experimental and calculated Raman spectra of the two molecules, we concluded that ESA transitions with either axial or equatorial transition dipole moments give rise to the Vis- and UV-bands, respectively. Two ESA bands could be fitted with the same time constants but showed different sensitivity to the ensuing structural dynamics in the excited state. The observed differences in the results for Mn_3 and Mn_6 allowed us to conclude that there is a sudden release of the JT distortion after LMCT excitation and this change gives rise to the vibrational wavepacket. The wavepacket dephases on a 300 fs timescale by coupling to other vibrational modes via IVR. Based on the global fit analysis, we conclude that the LMCT state decays into an intermediate state in less than 200 fs. This state in turn decays back to the ground electronic state with a 8 – 9 ps time constant.

Our experimental strategy of comparing molecules with either one or two Mn triangles allowed us to measure the JT distortion dynamics after photoexcitation of two Mn-based SMMs and find that the motion is governed by a coherent vibrational wavepacket. Design strategies for achieving ultrafast coherences in complex chemical systems for control and function-enhancement are actively being developed [22] and there have recently been several interesting observations in metal complexes, such as retention of vibrational coherence during intersystem crossing in $Cr(acac)_3$[42], metal-metal bond modulations in di-Pt(II) complexes[43] and in particular it has been shown that JT distortions, such as in Cu(I) complexes[44], are important.

Our work contributes to this field by demonstrating vibrational coherences in a molecule with as many as six metal ions. There is a peak in the Raman spectrum of the $Mn_{12}Ac$[45] SMM at 209 cm^{-1} and so it is possible that our approach is more general, which is supported by the observation of light-induced magnetisation changes in another Mn_{12} complex using continuous irradiation[46]. Our results therefore open up the possibility to study and control coherent magnetic interactions on the femtosecond timescale in a large range of SMMs.

Materials and Methods

The synthesis of the complexes has been described previously in Ref.[25] for Mn_6 and in Ref.[26] for Mn_3. For the transient absorption measurement, the Mn_6 and Mn_3 complexes were dissolved in ethanol. The concentration of the Mn_6 solution was 1.8 x 10^{-3} mol/l and the concentration of the Mn_3 complex in ethanol was 1.88 x 10^{-3} mol/l. A Starna flow cuvette with 0.2 mm pathlength was used for the TA measurements with a flow of 8 µl/min.

The TA setup is based on the apparatus described in ref. **[47].** As the pump beam, the second harmonic (400 nm) of a Coherent Legend Elite laser was used (pulse duration 120 fs and output 800 nm wavelength). The pump pulses were focused into the sample by a f = −500 mm concave mirror producing a spot size of 226 microns ($1/e^2$). The laser fluence was 3.3 mJ/cm^2. For the probe and reference beams 1.4 µJ/pulse of the 800 nm fundamental was focused with an f = 100 mm fused silica lens in a 5 mm thick CaF_2 plate, which was continuously moved in two dimensions, to produce a broadband white light continuum. The white light was collimated with an f = −100 mm concave mirror and the 800 nm fundamental was removed with a 720 nm cut off filter. The detected probe spectrum ranged from 320 to 720 nm. The white light beam was divided with a reflective metallic neutral density filter for probe and reference. The probe light was focused into the sample with an f = −500 mm concave mirror. The probe beam diameter in the sample was 105 µm ($1/e^2$). To avoid anisotropic signals, the pump-probe polarization angle was set to 54.7° (“magic angle”).

For controlling the time delay between pump and probe, a delay stage with mounted retroreflector was used. For each time delay 1000 spectra were collected. The whole procedure was repeated five times to get 5000 spectra in total for each delay position. A prism was used to disperse the white-light beams onto two fast CCD cameras from Entwicklungsbuero Stresing equipped with Hamamatsu S7031-0906 sensors with 512x58 active pixels. Full binning was used, where the 58 vertical pixel were binned, which allowed a synchronous read-out at 1 kHz for both probe and reference beams.

Raman spectroscopy of crystal grains of the Mn_3 and the Mn_6 complexes was performed on a Renishaw Raman microscope with a laser wavelength of 785 nm.

The geometry of $[Mn(III)_3O(Et\text{-}sao)_3(b\text{-}pic)_3(ClO_4)]$ has been optimised using the unrestricted DFT approach with the Perdew-Burke-Ernzerhof (PBE) functional[48] and the DKH-recontracted def2-SV(P) basis set[49] in the ground state with the Orca package[50]. Relativistic effects were taken into account within the Douglas Kroll Hess at second order (DKH2) approach[51-53] as implemented in Orca[54]. The frequency analysis of the optimised structure in the ground state of spin multiplicity M_s=13 showed one imaginary frequency ($-3.93\ cm^{-1}$). The corresponding normal mode involves the rotation of the phenyl groups around the N-Mn bond which is expected to occur along a flat potential energy curve. We therefore consider the geometry to be close enough from its minimum to conduct further studies.

Competing financial interests

The authors declare no competing financial interests.

Data availability

The authors confirm that all relevant data are included in the paper and/or its Supplementary Raw data are available on reasonable request from the authors.

Author contributions

FL performed the optical experiments and analysed the data and RMcN synthesized and characterised the samples under the supervision of RI. JE and TJP carried out the DFT calculations. FL, EKB and JOJ conceived the experiments and interpreted the results. FL and JOJ co-wrote the paper. All authors discussed the results and commented on the manuscript.

Acknowledgements

This work was supported by funding from the Royal Society of Edinburgh and the Carnegie Trust (Collaborative Research Grant). The authors thank M. D. Horbury and V. Stavros for allowing us to carry out preliminary measurements in their lab and assistance with these measurements. FL and JOJ thank A. Gromov for the help with the Raman spectrometer and E. Riedle for helpful advice with building the TA setup. JOJ is a Royal Society of Edinburgh/BP Trust research fellow. EKB thanks the EPSRC grants EP/P025986/1 and EP/N01331X/1. TJP and JE thank the EPSRC grants EP/R021503/1 and EP/P012388/1.

Bibliography

1 Christou, G., Gatteschi, D., Hendrickson, D. N. & Sessoli, R. Single-molecule magnets. *MRS Bull.* **25**, 66-71 (2000).

2 Cavallini, M. *et al.* Magnetic Information Storage on Polymers by Using Patterned Single-Molecule Magnets. *Angew. Chem. Int. Ed.* **44**, 888-892 (2005).

3 Bogani, L. & Wernsdorfer, W. Molecular spintronics using single-molecule magnets. *Nature Materials* **7**, 179-186 (2008).

4 Candini, A., Klyatskaya, S., Ruben, M., Wernsdorfer, W. & Affronte, M. Graphene Spintronic Devices with Molecular Nanomagnets. *Nano Lett.* **11**, 2634-2639 (2011).

5 Goodwin, C. A. P., Ortu, F., Reta, D., Chilton, N. F. & Mills, D. P. Molecular magnetic hysteresis at 60 kelvin in dysprosocenium. *Nature* **548**, 439-442 (2017).

6 Guo, F.-S. *et al.* A Dysprosium Metallocene Single-Molecule Magnet Functioning at the Axial Limit. *Angew. Chem. Int. Ed.* **56**, 11445-11449 (2017).

7 Guo, F.-S. *et al.* Magnetic hysteresis up to 80 kelvin in a dysprosium metallocene single-molecule magnet. *Science* 10.1126/science.aav0652 (2018).

8 McCusker, J. K. *et al.* Subpicosecond ^{1}MLCT $^{5}T_2$ intersystem crossing of low-spin polypyridyl ferrous complexes. *J. Am. Chem. Soc.* **115**, 298-307 (1993).

9 Monat, J. E. & McCusker, J. K. Femtosecond Excited-State Dynamics of an Iron(II) Polypyridyl Solar Cell Sensitizer Model. *J. Am. Chem. Soc.* **122**, 4092-4097 (2000).

10 Gawelda, W. *et al.* Ultrafast Nonadiabatic Dynamics of $[Fe^{II}(bpy)_3]^{2+}$ in Solution. *J. Am. Chem. Soc.* **129**, 8199-8206 (2007).

11 Consani, C. *et al.* Vibrational Coherences and Relaxation in the High-Spin State of Aqueous $[Fe^{II}(bpy)_3]^{2+}$. *Angew. Chem. Int. Ed.* **48**, 7184-7187 (2009).

12 Cannizzo, A. *et al.* Light-induced spin crossover in Fe(II)-based complexes: The full photocycle unraveled by ultrafast optical and X-ray spectroscopies. *Coord. Chem. Rev.* **254**, 2677-2686 (2010).

13 Mathonière, C., Lin, H. J., Siretanu, D., Clérac, R. & Smith, J. M. Photoinduced Single-Molecule Magnet Properties in a Four-Coordinate Iron(II) Spin Crossover Complex. *J. Am. Chem. Soc.* **135**, 19083-19086 (2013).
14 Feng, X. *et al.* Tristability in a Light-Actuated Single-Molecule Magnet. *J. Am. Chem. Soc.* **135**, 15880-15884 (2013).
15 Kamioka, H., Moritomo, Y., Kosaka, W. & Ohkoshi, S. Dynamics of charge-transfer pairs in the cyano-bridged Co^{2+}-Fe^{3+} transition-metal compound. *Phys. Rev. B* **77**, 180301 (2008).
16 Asahara, A. *et al.* Ultrafast dynamics of reversible photoinduced phase transitions in rubidium manganese hexacyanoferrate investigated by midinfrared CN vibration spectroscopy. *Phys. Rev. B* **86**, 195138 (2012).
17 Johansson, J. O. *et al.* Directly probing spin dynamics in a molecular magnet with femtosecond time-resolution. *Chem. Sci.* **7**, 7061–7067 (2016).
18 Dong, X., Lorenc, M., Tretyakov, E. V., Ovcharenko, V. I. & Fedin, M. V. Light-Induced Spin State Switching in Copper(II)-Nitroxide-Based Molecular Magnet at Room Temperature. *J. Phys. Chem. Lett.* **8**, 5587-5592 (2017).
19 Baniodeh, A. *et al.* Unraveling the Influence of Lanthanide Ions on Intra- and Inter-Molecular Electronic Processes in $Fe_{10}Ln_{10}$ Nano-Toruses. *Adv. Funct. Mater.* **24**, 6280-6290 (2014).
20 Caneschi, A. *et al.* Alternating current susceptibility, high field magnetization, and millimeter band EPR evidence for a ground S = 10 state in $[Mn_{12}O_{12}(CH_3COO)_{16}(H_2O)_4]$*2($CH_3COOH$)*4($H_2O$). *J. Am. Chem. Soc.* **113**, 5873-5874 (1991).
21 Sessoli, R. *et al.* High-spin molecules: $[Mn_{12}O_{12}(O_2CR)_{16}(H_2O)_4]$. *J. Am. Chem. Soc.* **115**, 1804-1816 (1993).
22 Scholes, G. D. *et al.* Using coherence to enhance function in chemical and biophysical systems. *Nature* **543**, 647–656 (2017).
23 Parois, P. *et al.* Pressure-induced Jahn-Teller switching in a Mn_{12} nanomagnet. *Chem. Commun.* **46**, 1881-1883 (2010).
24 Kaszub, W. *et al.* Ultrafast Photoswitching in a Copper-Nitroxide-Based Molecular Magnet. *Angew. Chem. Int. Ed.* **53**, 10636-10640 (2014).
25 Milios, C. J. *et al.* Toward a Magnetostructural Correlation for a Family of Mn_6 SMMs. *J. Am. Chem. Soc.* **129**, 12505-12511 (2007).
26 Inglis, R. *et al.* Twisting, bending, stretching: strategies for making ferromagnetic Mn^{III}_3 triangles. *Dalton Trans.*, 9157-9168 (2009).
27 Cremades, E. *et al.* Theoretical Methods Enlighten Magnetic Properties of a Family of Mn_6 Single-Molecule Magnets. *Inorg. Chem.* **48**, 8012-8019 (2009).
28 Bradley, J. M. *et al.* MCD spectroscopy of hexanuclear Mn(III) salicylaldoxime single-molecule magnets. *Dalton Trans.* **39**, 9904-9911 (2010).
29 Moro, F. *et al.* Addressing the magnetic properties of sub-monolayers of single-molecule magnets by X-ray magnetic circular dichroism. *Nanoscale* **2**, 2698-2703 (2010).
30 Milios, C. J. *et al.* A Record Anisotropy Barrier for a Single-Molecule Magnet. *J. Am. Chem. Soc.* **129**, 2754-2755 (2007).
31 Cheesman, M. R., Oganesyan, V. S., Sessoli, R., Gatteschi, D. & Thomson, A. J. Magnetically induced optical bi-stability of the molecular nanomagnet $Mn_{12}O_{12}(OOCMe)_{16}(H_2O)_4$ in an organic glass. *Chem. Commun.* **0**, 1677-1678 (1997).
32 Oppenheimer, S. M., Sushkov, A. B., Musfeldt, J. L., Achey, R. M. & Dalal, N. S. Diffuse optical excitations in Mn_{12}-acetate. *Phys. Rev. B* **65**, 054419 (2002).
33 McInnes, E. J. L. *et al.* Optical Detection of Spin Polarization in Single-Molecule Magnets $[Mn_{12}O_{12}(O_2CR)_{16}(H_2O)_4]$. *J. Am. Chem. Soc.* **124**, 9219-9228 (2002).
34 Domingo, N. *et al.* Magnetism of isolated Mn_{12} single-molecule magnets detected by magnetic circular dichroism: Observation of spin tunneling with a magneto-optical technique. *Phys. Rev. B* **69**, 052405 (2004).
35 *Absorption Spectra in the Ultraviolet and Visible Region*. Vol. 11 (Akademiai Kiado, Publishing House of the Hungarian Academy of Sciences, Budapest, 1968).
36 Brunold, T. C., Gamelin, D. R. & Solomon, E. I. Excited-State Exchange Coupling in Bent Mn(III)−O−Mn(III) Complexes: Dominance of the π/σ Superexchange Pathway and Its Possible Contributions to the Reactivities of Binuclear Metalloproteins. *J. Am. Chem. Soc.* **122**, 8511-8523 (2000).

37 Snellenburg, J., J., Laptenok, S., Seger, R., Mullen, K., M. & Van Stokkum, I., H.M. Glotaran: A Java-based graphical user interface for the R package TIMP. *Journal of Statistical Software* **49**, 1–22 (2012).
38 Juban, E. A. & McCusker, J. K. Ultrafast Dynamics of ^{2}E State Formation in $Cr(acac)_3$. *J. Am. Chem. Soc.* **127**, 6857-6865 (2005).
39 Polli, D. *et al.* Coherent orbital waves in the photo-induced insulator–metal dynamics of a magnetoresistive manganite. *Nature Materials* **6**, 643-647 (2007).
40 Beaud, P. *et al.* Ultrafast Structural Phase Transition Driven by Photoinduced Melting of Charge and Orbital Order. *Phys. Rev. Lett.* **103**, 155702 (2009).
41 Caviezel, A. *et al.* Femtosecond dynamics of the structural transition in mixed valence manganites. *Phys. Rev. B* **86**, 174105 (2012).
42 Schrauben, J. N., Dillman, K. L., Beck, W. F. & McCusker, J. K. Vibrational coherence in the excited state dynamics of $Cr(acac)_3$: probing the reaction coordinate for ultrafast intersystem crossing. *Chem. Sci.* **1**, 405-410 (2010).
43 Cho, S. *et al.* Coherence in Metal−Metal-to-Ligand-Charge-Transfer Excited States of a Dimetallic Complex Investigated by Ultrafast Transient Absorption Anisotropy. *J. Phys. Chem. A* **115**, 3990-3996 (2011).
44 Iwamura, M., Takeuchi, S. & Tahara, T. Ultrafast Excited-State Dynamics of Copper(I) Complexes. *Acc. Chem. Res.* **48**, 782-791 (2015).
45 North, J. M., van de Burgt, L. J. & Dalal, N. S. A Raman study of the single molecule magnet Mn_{12}-acetate and analogs. *Solid State Commun.* **123**, 75-79 (2002).
46 Rivière, E. *et al.* Magneto-optical control of a Mn_{12} nano-magnet. *J. Mater. Chem.* **20**, 7165-7168 (2010).
47 Megerle, U., Pugliesi, I., Schriever, C., Sailer, C. F. & Riedle, E. Sub-50 fs broadband absorption spectroscopy with tunable excitation: putting the analysis of ultrafast molecular dynamics on solid ground. *Appl. Phys. B* **96**, 215-231 (2009).
48 Perdew, J. P., Burke, K. & Ernzerhof, M. Generalized Gradient Approximation Made Simple. *Phys. Rev. Lett.* **77**, 3865-3868 (1996).
49 Weigend, F. & Ahlrichs, R. Balanced basis sets of split valence, triple zeta valence and quadruple zeta valence quality for H to Rn: Design and assessment of accuracy. *Phys. Chem. Chem. Phys.* **7**, 3297-3305 (2005).
50 Neese, F. Software update: the ORCA program system, version 4.0. *WIREs Comput. Mol. Sci.* **8**, e1327 (2018).
51 Wolf, A., Reiher, M. & Hess, B. A. The generalized Douglas–Kroll transformation. *J. Chem. Phys.* **117**, 9215-9226 (2002).
52 Douglas, M. & Kroll, N. M. Quantum electrodynamical corrections to the fine structure of helium. *Annals of Physics* **82**, 89-155 (1974).
53 Hess, B. A. Relativistic electronic-structure calculations employing a two-component no-pair formalism with external-field projection operators. *Phys. Rev. A* **33**, 3742-3748 (1986).
54 Neese, F. The ORCA program system. *WIREs Comput. Mol. Sci.* **2**, 73-78 (2012).